



# HEPATIC TUMOR ABLATION USING ELECTRIC CURRENT AND BIOHEAT TRANSFER MODEL: A 3D NUMERICAL ANALYSIS

R. Nasrin\* and Saima Akter Sawmpa

Department of Mathematics, Bangladesh University of Engineering and Technology, Dhaka-1000, Bangladesh.

\*Email: rehenamath@math.buet.ac.bd

## Abstract:

*This study examines a three-dimensional (3D) thermal-electric model comprising a hepatic tissue, four small radiofrequency probes, and a big blood vessel. The finite element method (FEM) is used to determine the distribution of tissue temperature during radiofrequency (RF) hepatic tumor ablation. The aim is to pinpoint the specific heated cells targeted for elimination and safeguard the neighboring healthy tissues. This will help in the effective and safe treatment of liver tumors. The mathematical model is simulated over 0 to 1000 seconds with a 22 to 50-volt voltage range. The iterative scheme shows good convergence. The temperature fields are analyzed and displayed graphically using iso-surfaces at 50°C with different time intervals. The graph depicts the heat distribution at the tip of one electrode arm over time. It demonstrates the temperature changes at a fixed voltage and various voltages during tumor ablation. Based on the RF simulation results, the temperature rises as tumor ablation and electric voltage duration increase. The tumor cells are effectively destroyed at around 50°C using 22 volts over a 480-second heating period. This model could be a valuable tool for physicians to safely and efficiently treat tumors without harming healthy tissues.*

**Keywords:** Bioheat transfer; FEM; radiofrequency; electric current; hepatic ablation; malignant tumor

## NOMENCLATURE

$C_b$ (Jkg <sup>-1</sup> K <sup>-1</sup> )	Heat capacitance of blood	$Q_j$ (Am <sup>-3</sup> )	Current source
$E$ (Vm <sup>-1</sup> )	Electric field intensity	$V$ (V)	Electric Voltage
$J$ (Am <sup>-1</sup> )	Current density	<b>Greek symbols</b>	
$T$ (K)	Temperature	$\rho$ (kgm <sup>-3</sup> )	Tissue density
$T_0$ (K)	Initial temperature	$\rho_b$ (kgm <sup>-3</sup> )	Blood density
$T_b$ (°C)	Temperature of blood	$\omega_b$ (s <sup>-1</sup> )	Perfusion rate of blood
$Q_{ext}$ (Wm <sup>-3</sup> )	Heating at spatial	$\sigma$ (sm <sup>-1</sup> )	Electrical conductivity
$Q_{met}$ (Wm <sup>-3</sup> )	Heat source from metabolism	$\kappa$ (Wm <sup>-1</sup> K <sup>-1</sup> )	Thermal conductivity

## 1. Introduction

Liver tumors, also called hepatic tumors, represent abnormal proliferations of cells within or on the liver. Notably, the liver comprises various cell types, each susceptible to different forms of tumors. These tumors can be dangerous for the human body, with malignant tumors being cancerous. They develop when cells grow uncontrollably. The condition can become deadly if the cells proliferate and disperse unchecked. Malignant tumors have a rapid rate of spread and can impact distant parts of the body via the process known as metastasis. The cancerous cells that travel to other areas resemble the original tumor cells and can infiltrate and damage other organs. For example, lung cancer can lead to liver cancer if the cancerous cells spread from the lung to the liver. It often becomes a target for metastatic tumors originating from other organs, attributed to its significant blood flow and filtration capabilities. The most recommended treatments for hepatic tumors are surgery or transplantation. Nonetheless, approximately 80% of patients with liver cancer are unable to undergo surgery, mainly due to their poor health status and financial constraints. Many patients are not suitable for surgical intervention because of various factors, such as the presence of tumor size, its location in a primary vessel, matters with blood clotting, and multifocal sickness. Consequently, there is a growing need for innovative, minimally invasive techniques to treat liver defects. Focal ablative therapy has emerged as a method to address hepatic malignancies. Unlike traditional surgery, this approach does not require the removal of a complete section of the sigmoid colon or an entire lobe of the liver.

The most widely researched forms of relativeness are RF expression, cryoablation, and irreversible electroporation. Each modality and modality selection also includes general principles and techniques. Al-Sakree et al. (2007) highlighted that irreversible electroporation represented a novel and efficient approach to non-thermal ablation of tumors. Very common modes, overall practices, and unalterable electroporation techniques for removing tumor cells were discussed by Knavel and Brace (2013).

Radiofrequency ablation (RFA) represents a minimally invasive approach for treating primary and secondary malignant tumors. This method offers the benefits of minimized side effects and enhanced immune response when compared to alternative treatment options. The mathematical modeling of Shafirstein and Feng (2013) had a significant contribution to thermal medicine. Animal and clinical RFA treatments are effectively similar to surgery.

Hepatic tumors are a clinical problem with poor treatment outcomes, more needs to be learned to improve the treatment. The supervision of hepatocellular carcinoma's progressively common health issue was enlisted by Davis et al. (2008).

Hepatic tumors with RFA treatments seem to work, but more research is needed. Haemmerich and Wood (2006) tried to find an analytical resolution for RFA using a cooled electrode of cylindrical shape. Their solution depended on various parameters, such as providing mathematical tools for designing surgical procedures and validating other modeling techniques. Hall et al. (2015) investigated a few critical issues in the model hepatic RFA, like cell death, electrical parameters, perfusion, etc. Their study found that the dimensions of the 50°C isotherms were affected by the electrical properties of the tissue when the heat source was active, and by the thermal properties during the cooling phase. Romero-Mendez and Berjano (2017) found that hepatic RFA preserved normal tissue, especially heated tumor cells with low frequencies.

Mathematical models can accurately predict the clinical impact of irreversible electroporation on liver tissue. Researchers have successfully demonstrated a clear connection between the electric energy applied and the area of tissue ablation. This relationship is theoretically validated through experiments conducted 10 hours after the irretrievable electroporation procedure. Berjano (2006) described the most advanced theoretical modeling used in studying RFA techniques and the present limitations, especially those related to the lack of accurate characterization of the biological tissues. The epicardial fat layer severely inhibited RF current passage, thus reducing the effectiveness of the atrial wall RFA in Suarez et al. (2010). Gasselhuber et al. (2010) concluded that computational models might be needed to determine the relationship between heat exposure and pharmacokinetics to optimize the supply of drugs for complex interplays such as heat dissipation and chemotherapy in treating heat-based cancers. Trujillo and Berjano (2013) described various methods for modeling the temperature dependence of electrical and thermal conductivities of biological tissue in RFA, which had minimal impact on the calculated lesion diameter. Sung et al. (2016) already reported historical, theoretical, mathematical, and reviews of this kind of analysis in the literature about hepatic tumor ablation. A modeling outline was refined to evaluate macrophage connections in the tumor/lump microenvironment to determine their impact on tumor progression in Mahlbacher et al. (2018).

Simulation and computer models designed explicitly for RFA have proven extremely useful, as evidenced by research in references. Liu et al. (2006) provided valuable insights into the 'oven effect,' a phenomenon where tumors surrounded by cirrhotic liver or fatty tissues experience enhanced heating efficiency. Their study underscored the critical importance of considering both the characteristics of cancer and the surrounding tissues when evaluating the effectiveness of radiofrequency ablation. Adheyaju et al. (2012) suggested that the most effective electrode configurations could be identified through numerical modeling combined with the practical application of irreversible electroporation. Their process involved selecting the most suitable optimization algorithm to determine the optimal electrode placement. In their research, Pillai et al. (2015) utilized an *ex vivo* calf liver model to investigate the effects of different methods. Their findings indicated that microwave and bipolar RFA techniques are less susceptible to heat sink effects than the monopolar approach. They also highlighted the importance of electrode configuration in the distribution of the electric field. Additionally, the computational models mentioned in Rossmann et al. (2017) could accurately predict the spatial profile of drug delivery, offering a crucial tool for enhancing our understanding and optimizing drug delivery systems.

Some numerical models and simulation results have been made for hepatic tumor RFA. 3D analysis of FEM with RFA for hepatic tumors was performed by Tungitkusolmun et al. (2002). They showed that underdose sites

might be adjacent to blood vessels from which tumors might regenerate. Sometimes, personalized models developed from preoperative images could be utilized to conduct finite element analysis (FEA) for planning RFA. Haemmerich and Webster (2005) presented the results of a temperature-controlled, 3D FEM in their study of in-training assessment records (RITA) utilizing 30 electrodes. Kroger et al. (2006) incorporated a modified version of the electrostatic equation and the widely recognized bioheat transfer model to analyze their study's heat and electrical potential distributions. Those equations were nonlinearly arranged based on material parameters that changed with temperature, dehydration, and tissue loss. Wang et al. (2012) modeled a 3D image and used a tissue-mimicking breast phantom to validate RF interstitial tumor ablation.

RF electrodes perform best in the monopolar expandable electrode (MEE) and hybrid expandable electrode (HEE). Payne et al. (2011) executed multi-scale modeling based on images and validated RFA in liver tumors. Their study was particularly problematic in the liver, where large blood vessels submerged heat, dissipated - distributed heat, and shrank the size of the wound locally (the volume damaged by heat treatment); sufficient experience on the part of the physician was required to optimize heat treatment to prevent a recurrence. Zhang et al. (2015) found that 25-mm diameter target tissues could be eliminated, but 30-mm and 35-mm diameter target tissues could not. Mellal et al. (2016) demonstrated that a directional probe equipped with a curved cathode for heating could effectively eliminate malignant cells while preserving adjacent healthy tissues. The direction of the probe controls temperature expansion during tumor heat release and may be a new tool for cancer specialists to prepare an effective heat release. Fang et al. (2018) used the commercial expandable electrode (CEE) to evaluate the effectiveness of complete tumor removal of RF electrodes designed to eradicate a large liver tumor with a diameter of 3.5 cm.

Very recently, Wang et al. (2023) reviewed the current state, challenges, and prospects of RFA in treating hepatocellular carcinoma. A study conducted by Qu et al. (2023) examined the use of anesthesia in liver tumor ablation from 1999 to 2022, quantitatively. Their study concluded that the use of anesthesia gained significant attention as liver tumor ablation was advanced. The findings of this bibliometric study provide valuable insights into the current state and trends of anesthesia in liver tumor ablation research. Başkak et al. (2023) studied the local recurrence of malignant hepatic tumors after thermal ablation therapy. Their findings revealed that the primary risk factors for local recurrence were a tumor diameter larger than 3 cm and intrahepatic distant recurrence. In contrast, other parameters showed no significant relationship to the local recurrence rate.

The literature reviewed indicates a lack of research on hepatic tumor ablation in several areas. The gaps in the existing literature are as follows:

- ❖ Integration of electric current and bioheat transfer models are not used.
- ❖ Computational model validation with experimental data is not available.
- ❖ Optimization of ablation parameters is not studied.
- ❖ Patient-specific factors have not been incorporated into the research.
- ❖ Novel ablation techniques have not yet been explored.

Additional research is necessary to address gaps in the literature and enhance our comprehension of hepatic tumor ablation. Researchers can contribute to improving hepatic tumor ablation, thus providing personalized treatment and enhancing patient outcomes. However, continuous numerical analysis is crucial to ensure consistent heat distribution from the electrode within the liver, covering healthy cells, tumor cells, the blood circulation system, and blood vessels. These issues have not been established in the above literature, which has motivated the present study. In this research, temperature thresholds of healthy tissue and tumor cells along blood vessels using time and voltage variation are investigated numerically for hepatic ablation.

This research develops a 3D thermal-electric model for radiofrequency hepatic tumor ablation. It includes a detailed representation of the probe, hepatic tissue, and blood vessels. The model uses fem to determine temperature distribution, which is crucial in identifying targeted cells for elimination while safeguarding healthy tissues. The study suggests that a temperature of 50°C, 22 volts over 480 seconds, effectively eliminates tumor cells. The model can potentially be a valuable tool for physicians in developing treatment strategies for hepatic tumor ablation.

## 2. Physical Configuration

The research achieves local heating through the insertion of a four-armed electric probe. This probe is composed of a primary rod known as a trocar. The tip and base of the trocar each have a radius of 0.91 mm and are positioned 10 mm and 50 mm away from the plane, respectively. The electrode arm, which extends from the trocar and has a radius of 0.27 mm, is insulated along its length, except in areas near the arms, allowing electric current to pass through. This design creates an electric field within the tissue when an electric current is applied through the probe. The electric field intensity is most incredible near the probe, resulting in significant resistive heating, particularly everywhere the electrode arms due to the robust electric field. For modeling purposes, the body tissue is represented as a substantial cylinder, measuring 120 mm, and 50 mm in height and radius, respectively. The tumor is situated near the center of the cylinder and shares identical thermal properties with the nearby tissue. The design thoughtfully positions the probe along the cylinder's central axis, ensuring its electrodes effectively encompass the tumor region.

Tumor cells are a huge necessity for nutrients and oxygen. Thus, increasing tumors depends on the concurrent development of vessels, which creates a source system for tumors. A better understanding of blood vessel growth (both normal and abnormal settings) may be helpful for us in identifying effective therapeutics for the tumor to stop vessel development more successfully. In our computational model, we incorporate a significant blood vessel with a 5 mm radius and positioned 120 mm from the reference plane. This is depicted in Figure 1, showing a four-armed electric probe situated adjacent to a substantial blood vessel at the center [COMSOL Multiphysics 4.3]. The objective of this treatment is twofold: primarily, to eradicate tumor cells located at the cylinder's core, and secondarily, to avoid damaging the healthy liver cells, which are represented as a cylinder surrounding the tumor [COMSOL Multiphysics 4.3].

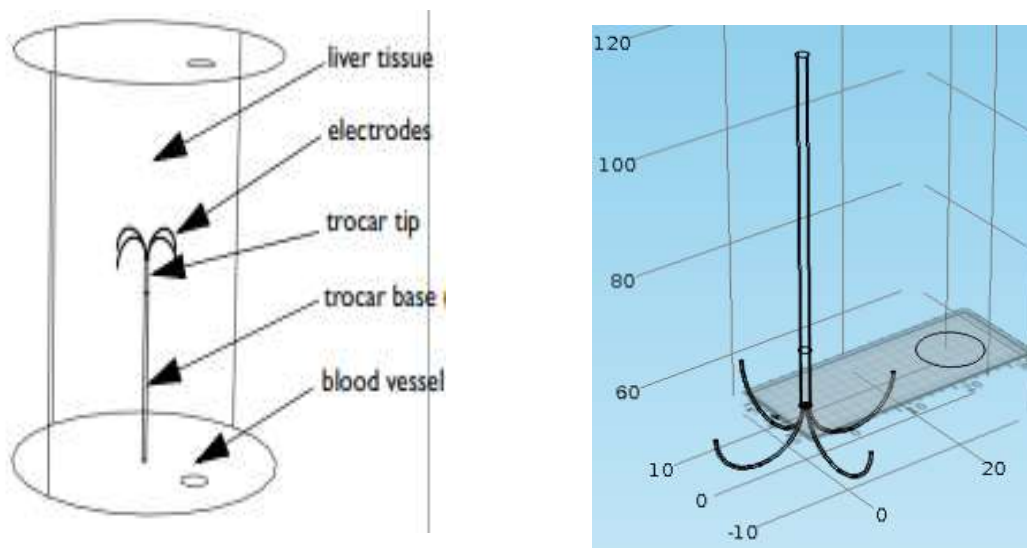


Figure 1: (a) Liver tissue with electric probe at the liver center (tumor location) and (b) computational domain [COMSOL Multiphysics 4.3].

The RF expandable electrode (probe trocar) is designed to comprise three parts (i.e., an insulated shaft, changing shaft, and hooks). The probe contains four curved hooks that can be deployed from the electrode hollow in an umbrella-like shape, according to Tungitkusolmun et al. (2002), as shown in Figure 2.

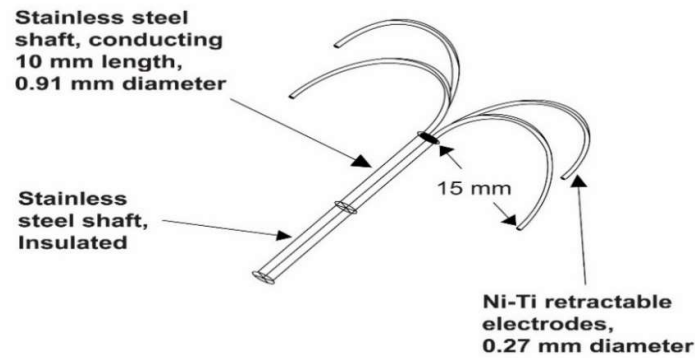


Figure 2: RF probe structure [Tungitkusolmun et al. (2002)].

Figure 3(a-b) depicts the 3D geometry, where we present a liver tissue in cylindrical form through a 3D visualization alongside a detailed zoomed-in view. Techniques involving probes have been utilized for the extraction of suspected tumors.

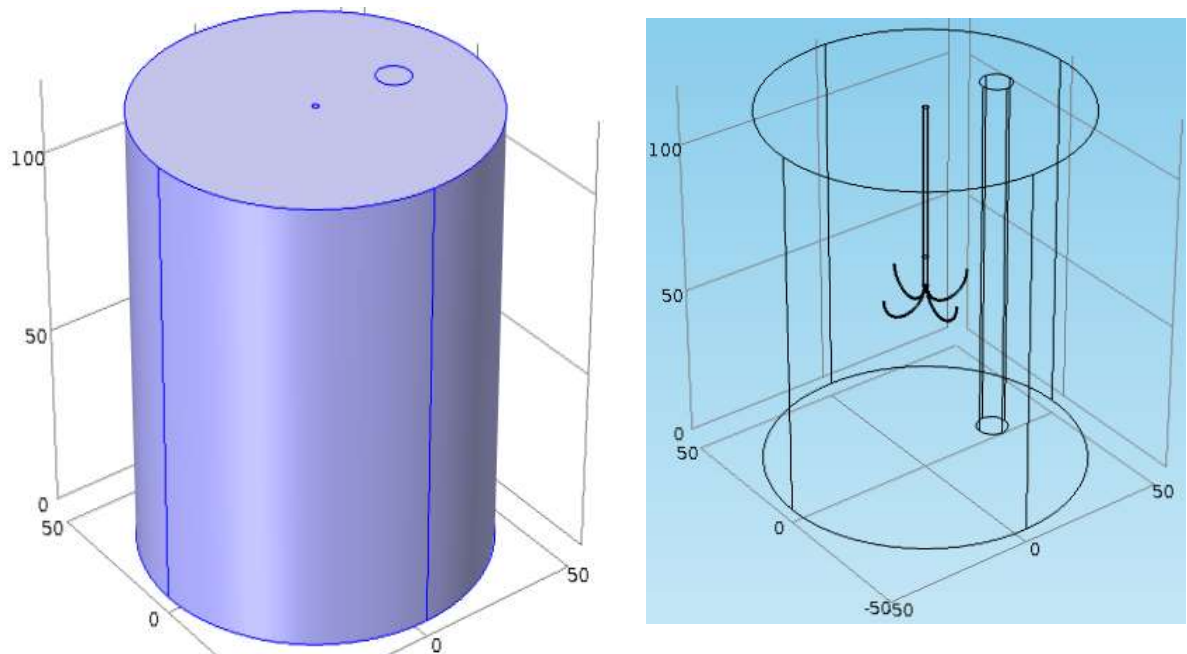


Figure 3: 3D geometry - (a) exterior perspective, and (b) interior perspective [COMSOL Multiphysics 4.3].

### 3. Mathematical Formulation

The bioheat equation regulates heat transfer within tissues and different components of the probe. It assumes a consistent temperature of 310.15 Kelvin at the cylinder's external borders and the blood vessels' walls. Furthermore, there is a continuous heat flux across all other boundaries. Regarding electrical potential, it is set at 22 volts at the electrode and 0 volts at the outer boundaries of the cylinder (Surita et al. (2012), Mellal et al. (2016), COMSOL Multiphysics 4.3).

The fundamental bioheat equation applicable to liver tissue and the probe, excluding blood (Surita et al. (2012), Mellal et al. (2016), COMSOL Multiphysics 4.3):

$$\rho C \frac{\partial T}{\partial t} + \nabla \cdot (-\kappa \nabla T) = \rho_b C_b \omega_b (T_b - T) + Q_{met} + Q_{ext} \quad (1)$$

Here  $C \rightarrow$  tissue specific heat ( $\text{Jkg}^{-1}\text{K}^{-1}$ ),  
 $\rho_b \rightarrow$  blood density ( $\text{kgm}^{-3}$ ),  
 $C_b \rightarrow$  blood specific heat ( $\text{Jkg}^{-1}\text{K}^{-1}$ ),  
 $\kappa \rightarrow$  tissue thermal conductivity ( $\text{Wm}^{-1}\text{K}^{-1}$ ),  
 $\omega_b \rightarrow$  blood perfusion rate ( $\text{s}^{-1}$ ),  
 $\rho \rightarrow$  tissue density ( $\text{kgm}^{-3}$ ),  
 $Q_{\text{met}} \rightarrow$  heat sources from metabolism ( $\text{Wm}^{-3}$ ),  
 $T_b \rightarrow$  blood temperature ( $^{\circ}\text{C}$ ), and  
 $Q_{\text{ext}} \rightarrow$  spatial heating ( $\text{Wm}^{-3}$ ).

In this study, the heat transfer coefficient,  $Q_{\text{met}}$ , is considered negligible due to its minimal impact. The outer heat originates from the energy produced by the electric current:

$$Q_{\text{ext}} = \mathbf{J} \cdot \mathbf{E} \quad (2)$$

Here  $\mathbf{E} \rightarrow$  intensity of electric field ( $\text{Vm}^{-1}$ ), and  
 $\mathbf{J} \rightarrow$  current density ( $\text{Am}^{-2}$ ).

Thus, equation (1) becomes for liver tissue:

$$\rho C \frac{\partial T}{\partial t} + \nabla \cdot (-\kappa \nabla T) = \rho_b C_b \omega_b (T_b - T) + \mathbf{J} \cdot \mathbf{E} \quad (3)$$

The bioheat equation accounts for heat transfer in various probe components, using the correct values for specific heat and thermal conductivity. For these components, all the terms on the right-hand side of the equation (3) become zero:

$$\rho C \frac{\partial T}{\partial t} + \nabla \cdot (-\kappa \nabla T) = 0 \quad (4)$$

The governing equation for the conservation of electric current (Surita et al. (2012), COMSOL Multiphysics 4.3):

$$-\nabla \cdot \mathbf{J} = \mathbf{Q}_j \quad (5)$$

Here  $\mathbf{J} = \sigma \mathbf{E} - \mathbf{J}^e$  and  $\mathbf{E} = \nabla V$

So, the equation (5) takes the following form:

$$-\nabla \cdot (\sigma \nabla V - \mathbf{J}^e) = \mathbf{Q}_j \quad (6)$$

Here  $\mathbf{J}^e \rightarrow$  externally generated current density ( $\text{Am}^{-2}$ ),

$V \rightarrow$  potential (V),

$\sigma \rightarrow$  electrical conductivity ( $\text{Sm}^{-1}$ ), and

$\mathbf{Q}_j \rightarrow$  current source ( $\text{Am}^{-3}$ ).

In this case, both  $\mathbf{Q}_j$  and  $\mathbf{J}^e$  are set to zero.

Consequently, the governing equation can be simplified into the following form:

$$-\nabla \cdot (\sigma \nabla V) = 0 \quad (7)$$

The border criteria for the bioheat model (Surita et al. (2012), Mellal et al. (2016), COMSOL Multiphysics 4.3):

$T = T_b \rightarrow$  liver outer boundaries

$\mathbf{n} \cdot (\kappa \nabla T) = 0 \rightarrow$  interior boundaries

$T_0 = 310.15 \text{ K} \rightarrow$  initial temperature.

The boundary conditions for the electric current model (Surita et al. (2012), COMSOL Multiphysics 4.3):

$V = 0 \rightarrow$  trocar base, liver outer boundaries, blood vessel

$V = V_0 \rightarrow$  electrode boundaries, trocar tip

$\mathbf{n} \cdot \mathbf{J} = 0 \rightarrow$  other boundaries

### 3.1 Properties

The thermophysical characteristics of blood, such as electric potential and temperature, are referenced from (Surita et al. (2012), Mellal et al. (2016), COMSOL Multiphysics 4.3) and presented in Table 1. The characteristics of the three-dimensional model are documented in Table 2. Additionally, it is assumed that the characteristics of liver tissue remain unaltered regardless of temperature changes.

Table 1: Thermophysical characteristics (Surita et al. (2012), Mellal et al. (2016), COMSOL Multiphysics 4.3).

Name	Expression	Description
$\omega_b$	$0.0064 \text{ s}^{-1}$	Perfusion rate
$T_b$	$37^\circ\text{C}$	Temperature
$T_0$	$310.15 \text{ K}$	initial temperature
$V_0$	$22 \text{ V}$	Voltage, electrical

Table 2: Thermal and electric properties (Surita et al. (2012), Mellal et al. (2016), COMSOL Multiphysics 4.3).

Unit	Name	Trocar tip	Blood	Trocar base	Liver	Electrode
$\text{Jkg}^{-1}\text{K}^{-1}$	Capacitance of heat, $C_p$	132	4180	$1\text{e-}5$	3600	840
$\text{Wm}^{-1}\text{K}^{-1}$	Thermal conductivity, $\kappa$	71	0.543	0.026	0.512	18
$\text{Kgm}^{-3}$	Density, $\rho$	21500	1000	70	1060	6450
$\text{Sm}^{-1}$	Electric conductivity, $\sigma$	$4\text{e}6$	0.667	1045	0.333	$1\text{e}8$

## 4. Computational Process

Utilizing the Galerkin weighted residual technique within the FEM framework of Dechaumphai (1999), the solution domain is divided into a mesh comprising four distinct element types: triangular, quadrilateral, edge, and vertex. This technique facilitates the expansion and solution of unknown temperature and electric potential variables at each nodal point, ensuring precise calculations at every degree of freedom. The unsteady solution is obtained at 0 s to 1000 s to find the time-dependent temperature field. At every 60 seconds, the temperature distribution is observed to determine the time needed to achieve temperature 323 K, at which tumor/cancer tissues may be eradicated. The comparative mistake for individual dependent variables between successive repetitions is logged as lower than 0.0001.

### 4.1 Finite element meshing

Figure 4 illustrates the computational area's finite element (FE) meshing, which employs non-uniform tetrahedral and triangular elements. In this detailed meshing approach, our computational area comprises four unique element types: tetrahedral, triangular, edge, and vertex elements. These element quantities are as follows: tetrahedral elements number 72052, triangular elements at 5290, edge elements at 976, and vertex elements at 76, respectively.

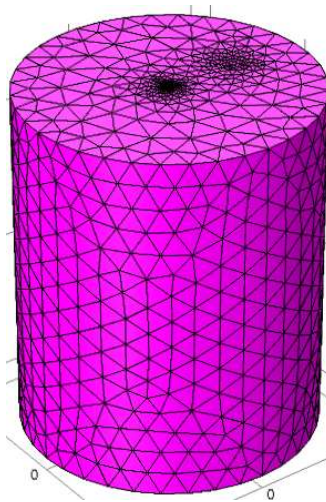


Figure 4: FE mesh generation for 3D space.

The total size of the element is given as 78394. In this finely meshed model, the sizes for the minimum and average elements are reported as 0.002334 meters and 0.7004 meters, respectively. The ratio of the element volume is noted to be 9.668E-6. The mesh volume is calculated to be 938700.0 cubic millimeters. Additionally, the resolution in narrower regions is identified as 0, indicating no resolution, while the maximum rate at which the element size increases is 5.35.

## 4.2 Coding check

The code validation of the current numerical simulation of temperature distribution of the bioheat transfer model of human body cells and blood flow is shown in detail in Nasrin et al. (2020, 2022) and is not repeated here.

## 5. Outcomes with Discussions

This study presents a detailed mathematical investigation focused on managing temperatures in liver tumor tissues using electrodes. It leverages electrical currents and bioheat models to achieve precise temperature control. It meticulously examines how variations in time, ranging from 0 to 1000 seconds, and electric voltage, from 25 to 50 volts, influence temperature thresholds within the tissue.

### 5.1 Influence of time

The temperature fields of the healthy liver tissue, electric probe, and tumor cell (located at the center of the liver) with 22 V for various times like 60 s, 120 s, 180 s, 240 s, 300 s, 360 s, 420 s, and 480 s are depicted in Figure 5 (i-viii).

The duration of heating must be carefully controlled to achieve optimal treatment outcomes while ensuring safety, efficacy, and patient comfort during hepatic tumor ablation using electric current. The plots of temperature fields in Figure 5 play a crucial role in analyzing the thermal properties of systems and are vital in advancing research in fields such as engineering, physics, and environmental science. In this case, the wound exhibits features resembling a mushroom, slightly protruding due to the cooling effect on the blood vessels. Each sub-figure in Figure 5 illustrates the temperature distribution following 60 seconds of heating, indicating a gradual increase in temperature every 60 seconds. The temperature surrounding the electrode, which is positioned at the center of the tumor, experiences a rise. A considerable temperature variation is observed within the time frame from 60 seconds to 300 seconds. Moreover, a marked change in temperature occurs between 360 seconds and 480 seconds. Here, the color of the temperature bar changes from red to white, representing inferior to a higher temperature.

Figure 6 (i-viii) shows the iso-surfaces of the electric probe and tumor cell at 50°C for various times as the 60 s, 120 s, 180 s, 240 s, 300 s, 360 s, 420 s, 480 s with 22 V. The iso-surface plots of Figure 6 enhance the presentation of research findings by providing a clear visual representation, thereby elevating the overall impact and understanding of the study. The malignant tissue damage is minimal after heating for 1 minute. However, with the extension of the ablation time, there is a marked increase in tissue damage.

The area where cancer cells die becomes identifiable upon reaching a temperature of 50°C at various intervals. Figure 6 (viii) demonstrates that cancer cells begin to die approximately 8 minutes after the temperature hits 50°C.

Figure 7 (i-viii) shows the iso-surfaces of the electric probe and tumor cell with 480 s, 22 V for temperature variations 37°C, 38°C, 39°C, 41°C, 43°C, 45°C, 47°C, 50°C. The temperature in the hepatic tumor ablation system is a critical factor that impacts various aspects of treatment. It affects the effectiveness of tumor destruction, surrounding tissue safety, the size of the thermal damage area, and the patient's comfort and recovery. By carefully controlling the heating temperature, clinicians can achieve better treatment outcomes while reducing the risks to the patient. The malignant cell size significantly diminishes when exposed to a temperature of 37°C for 480 seconds. This reduction results from the heat delivered directly to the tissue through an electrode.

Figure 8 illustrates the variation in heat distribution across different time intervals, ranging from 0 to 1000 seconds, with a steady voltage of 22 V maintained at the tip of one of the electrodes. Here, the electric probe has four arms (hooks), and the temperature distribution in all these arms is uniform. That's why we are showing the temperature threshold versus time for one arm of the RF probe here. The temperature rises quickly until it reaches 80°C within the 50 s. Subsequently, the rate of temperature increase decelerates, eventually reaching a steady state of approximately 94°C at the 480-second mark. Beyond this point, there is no notable change in the temperature at the electrode's tip.

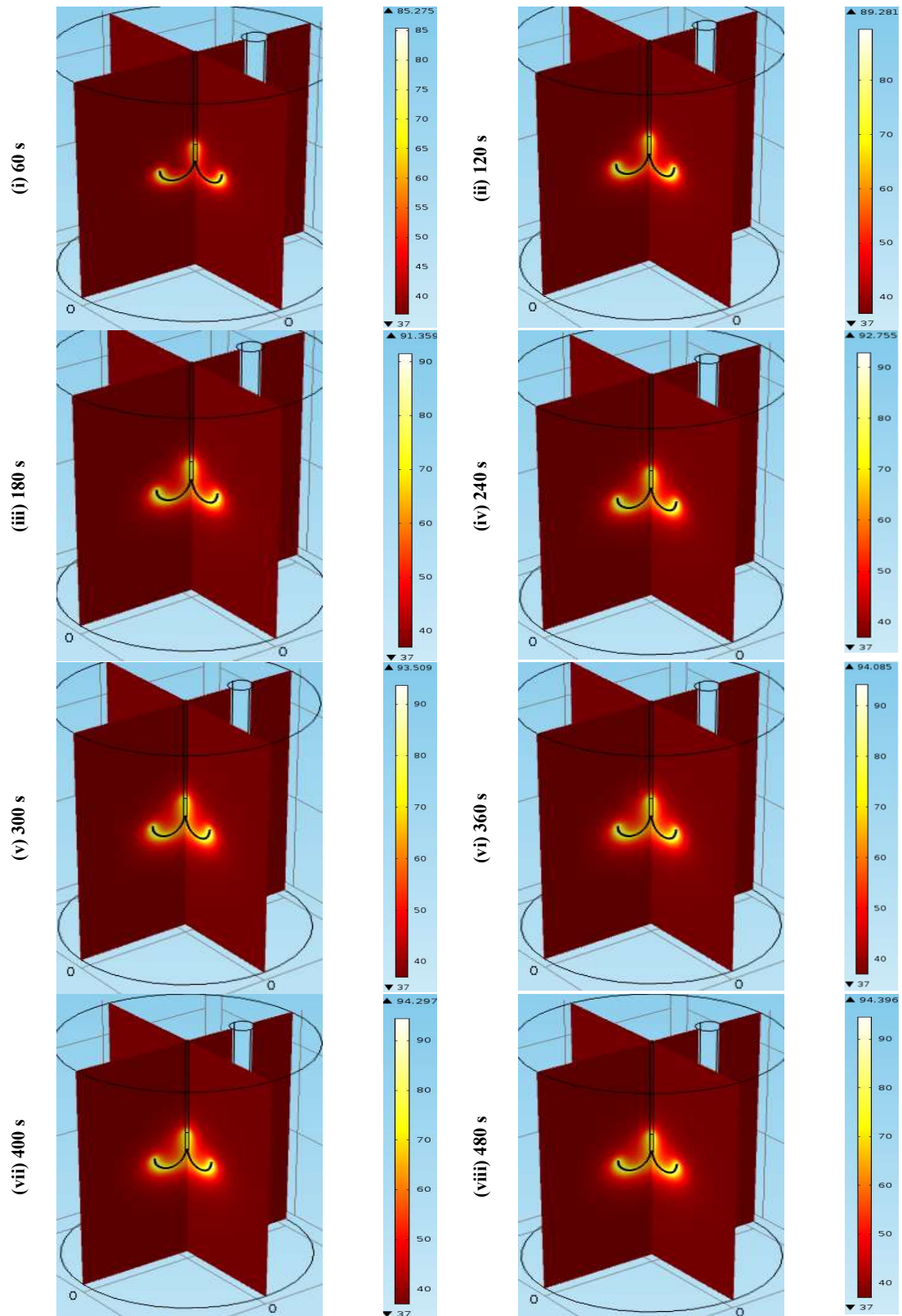


Figure 5: Temperature fields due to time variation at 22 V (i) 60 s, (ii) 120 s, (iii) 180 s, (iv) 240 s, (v) 300 s, (vi) 360 s, (vii) 420 s, (viii) 480 s.

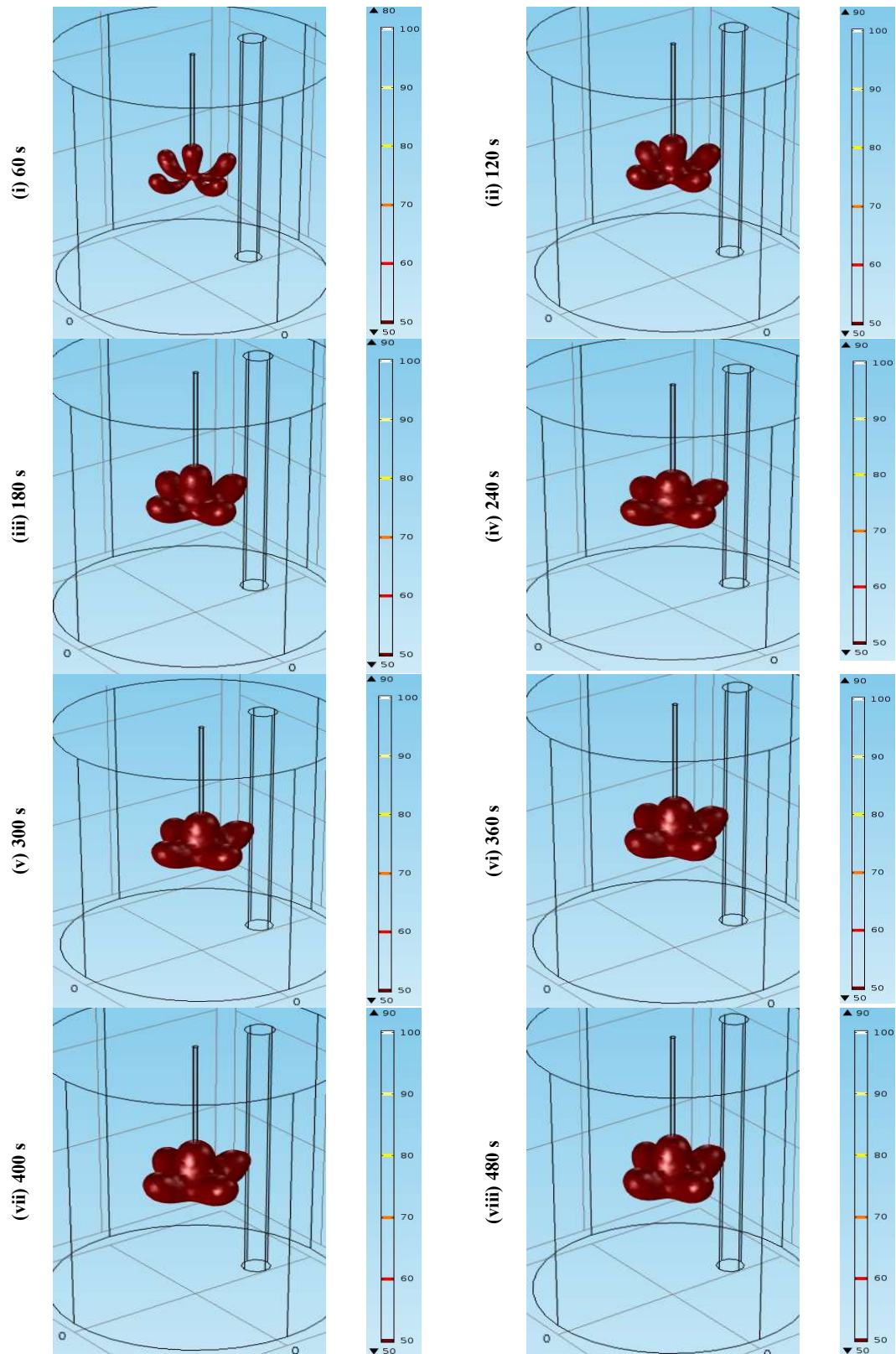


Figure 6: Iso-surface plots for various times (i) 60 s, (ii) 120 s, (iii) 180 s, (iv) 240 s, (v) 300 s, (vi) 360 s, (vii) 420 s, (viii) 480 s with 22 V and 50°C.

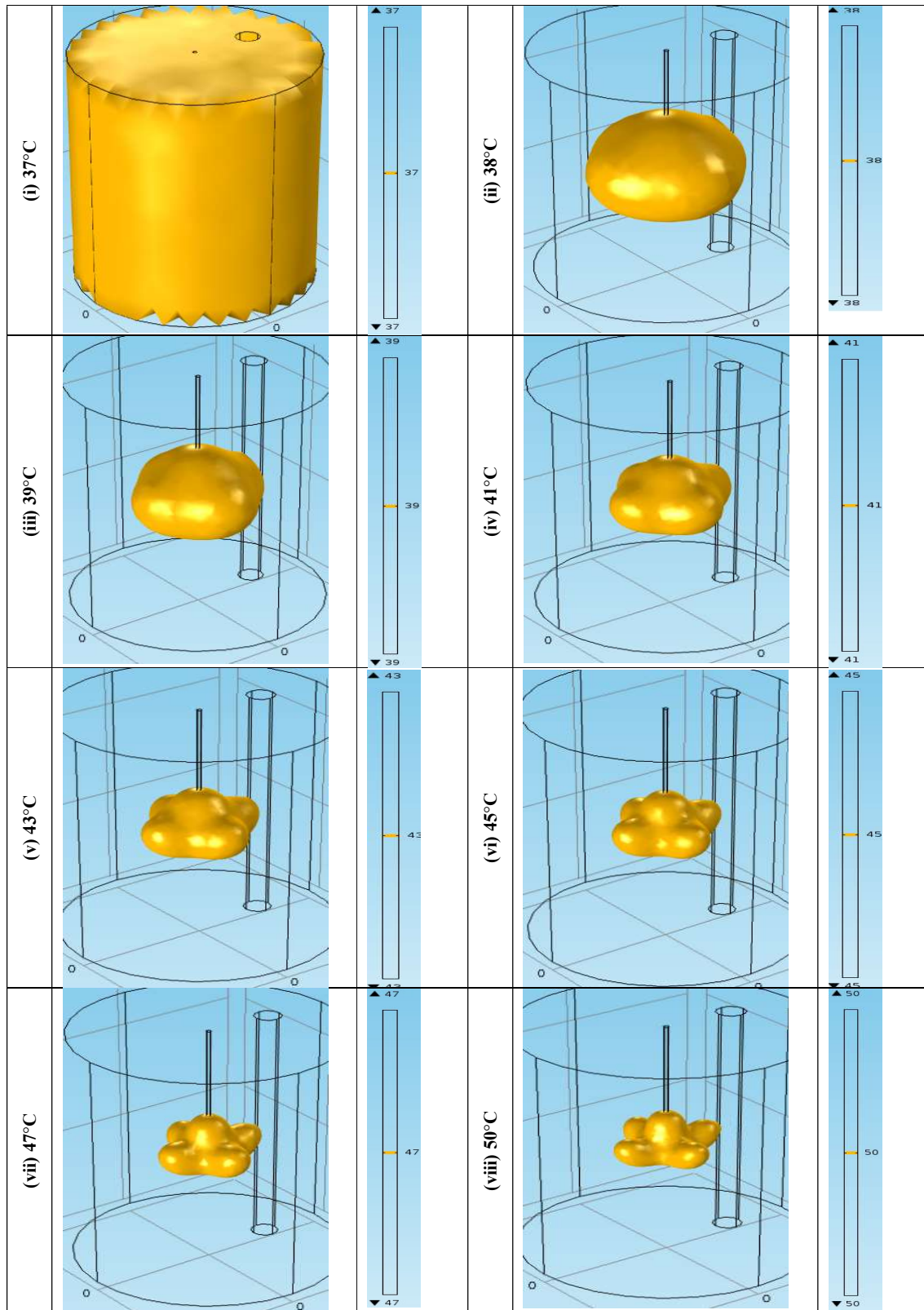


Figure 7: Iso-surface plot with 480 s and 22 V for temperature variation (i) 37°C, (ii) 38°C, (iii) 39°C, (iv) 41°C, (v) 43°C, (vi) 45°C, (vii) 47°C, (viii) 50°C.

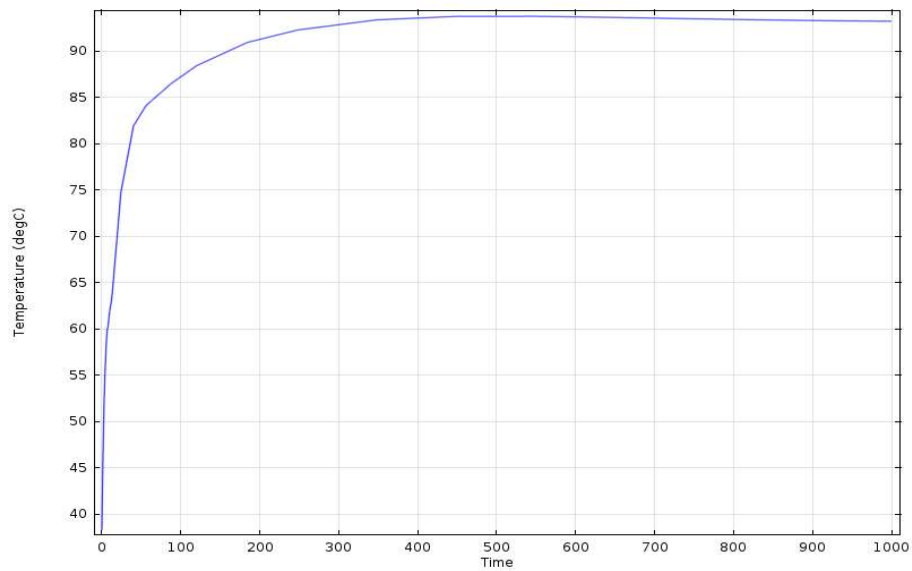


Figure 8: Temperature against time at the electrode tip with 22 V.

## 5.2 Influence of electrical voltage

Figure 9, parts (i-vi), presents the temperature distributions observed at various electric voltages, specifically 25 V, 30 V, 35 V, 40 V, 45 V, and 50 V, over a constant duration of 480 seconds within healthy liver tissues and tumor cells. The impact of electric voltage is essential for achieving effective tumor ablation while minimizing damage to surrounding healthy tissue. The voltage parameters, which include amplitude, duration, and frequency, are meticulously controlled to ensure precise and controlled tumor destruction. Furthermore, imaging guidance, such as ultrasound or computed tomography (CT) scans, is often used to monitor the ablation process in real time, which provides accurate ablation probe placement and treatment effectiveness assessment. Observations indicate that the liver's central region, housing tumor tissue, exhibits elevated temperatures. This increase is due to applying an electric current via a probe, which generates an electric field within the tissue. The heating, primarily resistive, is most intense around the probe's electrode arms due to the potent electric field they produce. Observations indicate that an increase in electric voltage leads to a corresponding rise in temperature. Notably, the highest temperatures are recorded at the center of the tissue. The temperature increment is directed towards the cathode, facilitating tumor removal. Significant temperature variations are directly linked to changes in electric voltages. As the electric voltage escalates, the central region of the tissue experiences sustained high temperatures, making the core area visibly hotter on the surface plot. Here, the color of the temperature bar changes from blue to red, representing the minimum to maximum.

Figure 10 illustrates the relationship between temperature and time at the tip of an electrode arm exposed to various electric voltages: 25 V, 30 V, 35 V, 40 V, 45 V, and 50 V. The graph spans a timeframe from 0 seconds to 600 seconds. It reveals how temperature changes over time at each voltage level, demonstrating that the temperature observed at 25 V is notably lower than that at 50 V. Figure 10 illustrates the correlation between temperature and time as the electric voltage varies. It is observed that lower electric voltages are associated with lower temperatures. Specifically, when the electric voltage is adjusted from 25 V to 50 V, there is a swift increase in temperature, which stabilizes after 400 seconds. This graph effectively demonstrates the impact of varying electric voltages on temperature. As the electric voltage increases, so does the temperature. From this figure, anyone can easily understand that choosing a proper electric voltage from 25 V to 50 V is unsuitable for our healthy tissue. The electrode tip's rising temperature becomes exuberantly high and unacceptable for the human body. Also, a rise in temperature above 100°C is not allowed in clinical practice due to tissue charring and carbonization as this would restrict the heat transfer from the electrode surface to the tissue far from the electrode surface. This temperature rise would severely impact the outcome of the procedure. That's why, from this analysis, we can select the proper amount of electric voltage, not more than 22 V.

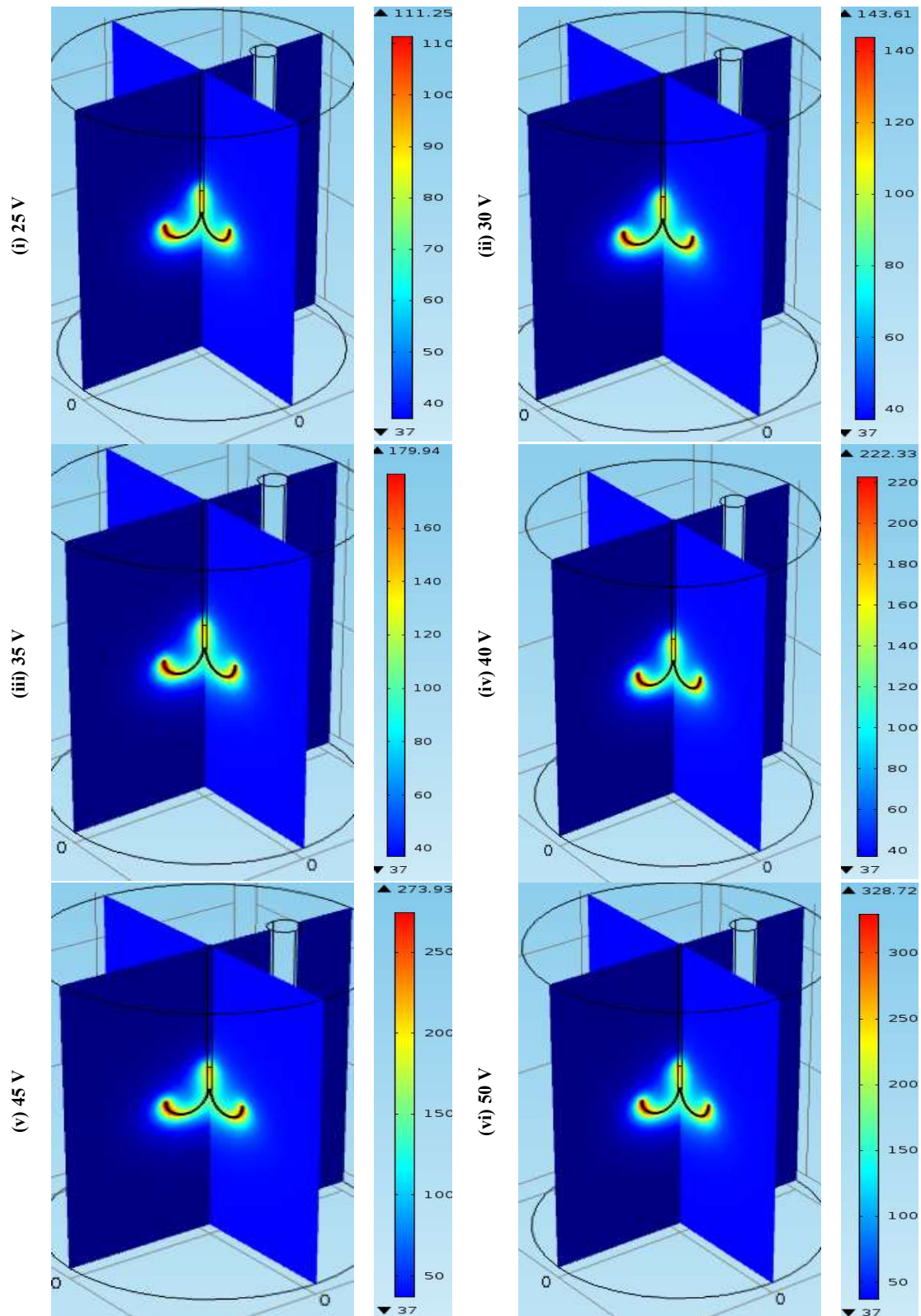


Figure 9: Temperature fields for electric voltage variations (i) 25 V, (ii) 30 V, (iii) 35 V, (iv) 40 V, (v) 45 V, and (vi) 50 V with 480 s.

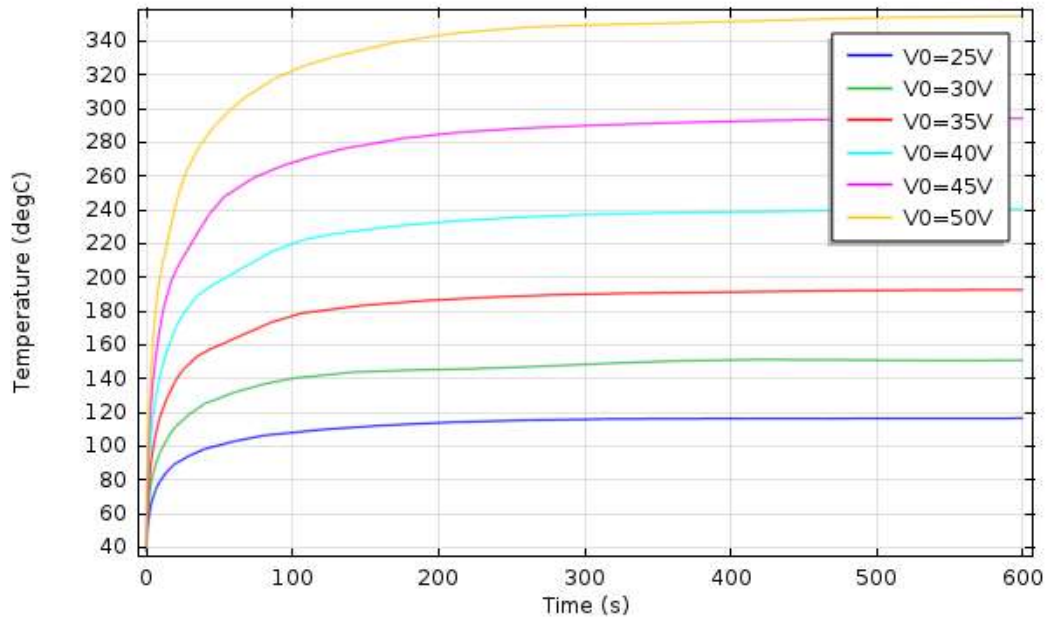


Figure 10: Temperature against time at the electrode tip due to various electric voltages.

## 5. Conclusions:

The research focuses on applying medical technology to a large liver blood vessel. It discusses a temperature threshold that can kill tumor cells while minimizing damage to healthy cells, particularly those in the liver. The threshold is determined by variations in time, voltage, and distance from the electrode. Our numerical simulation analyzes how the temperature near the electrode inside the tumor cell rises over time.

The major conclusions from this research are as follows:

- An increased temperature from 37°C to 94°C is observed at the electrode tip during the first 1000 seconds of growth at 22V.
- The annihilation of tumor tissue increases as the temperature rises by 50°C for 0 to 480 seconds.
- The size of malignant cells significantly reduces when the temperature increases from 37°C to 50°C.
- It takes approximately 480 seconds to kill the tumor cells at 22 volts.

In the future, researchers may investigate which parts of the tumor and liver tissues are most at risk of not surviving. They may also compare temperature threshold levels for healthy cells and tissues related to blood vessel circulation. This could help physicians remove malignant liver tumors without harming healthy tissue. The process involves implanting a small RF probe to create a regional heat source.

We have discovered that using a more refined mesh element for our calculations causes difficulties in achieving convergence due to the larger number of mesh elements required. Unfortunately, we face challenges in conducting a parametric sweep due to our current computer configuration's lack of laboratory resources. We believe combining numerical and experimental work could lead to better results, but we do not have access to a laboratory facility now.

## References

Al-Sakree, B., Andre, F., Bernat, C., Connault, E., Opolon, P., Davalos, R.V., Rubinsky, B. and Mir, L.M. (2007): Tumor ablation with irreversible electroporation, PLOS ONE, Vol. 2(11), e1135. <https://dx.doi.org/10.1371/journal.pone.0001135>

- Knavel, E.M. and Brace, C.L. (2013): Tumor ablation: common modalities and general practices, *Techniques in Vascular and Interventional Radiology*, Vol. 16(4), pp. 192-200. <https://dx.doi.org/10.1053/j.tvir.2013.08.002>
- Shafirstein, G. and Feng, Y. (2013): The role of mathematical modeling in thermal medicine, *Int. J. of Hyperthermia*, Vol. 29(4), pp. 259-261. <https://dx.doi.org/10.3109/02656736.2013.800999>
- Davis, G.L., Dempster, J., Meler, J.D., Orr, D.W., Walberg, M.W., Brown, B., Berger, B.D., O'Connor, J.K., Goldstein, R.M. (2008): Hepatocellular carcinoma: Management of an increasingly common problem, *Bayl. Univ. Med. Cent. Proc.*, Vol. 21(3), pp. 266–280, 2008. <https://dx.doi.org/10.1080/08998280.2008.11928410>
- Haemmerich, D. and Wood, B.J. (2006): Hepatic radiofrequency ablation at low frequencies preferentially heat tumor tissue, *Int. J. of Hyperthermia*, Vol. 22(7), pp. 563-574. <https://dx.doi.org/10.1080/02656730601024727>
- Hall, S.K., Ooi, E.H. and Payne, S.J. (2015): Cell death, perfusion, and electrical parameters are critical in models of hepatic radiofrequency ablation, *Int. J. of Hyperthermia*, Vol. 31(5), pp. 538-550. <https://dx.doi.org/10.3109/02656736.2015.1032370>
- Romero-Mendez, R. and Berjano, E. (2017): An analytical solution for radiofrequency ablation with a cooled cylindrical electrode, *Mathematical Probs. in Engg.*, Vol. 2017, Article ID 9021616 1, pp. 1-12. <https://dx.doi.org/10.1155/2017/9021616>
- Berjano, E.J. (2006): Theoretical modeling for radiofrequency ablation: state-of-the-art and challenge for the future, *Biomedical Engineering OnLine*, Vol. 5, Article number 24. <https://dx.doi.org/10.1186/1475-925X-5-24>
- Suarez, A.G., Hornero, F. and Berjano, E.J. (2010): Mathematical modeling of epicardial RF ablation of atrial tissue with overlying epicardial fat, *The Open Biomedical Engineering Journal*, Vol. 4, pp. 47-55. <https://dx.doi.org/10.2174/1874120701004020047>
- Gasselhuber, A., Dreher, M.R., Negussie, A., Wood, B.J., Rattay, F. and Haemmerich, D. (2010): Mathematical spatio-temporal model of drug delivery from low temperature-sensitive liposomes during radiofrequency tumor ablation, *International Journal of Hyperthermia*, Vol. 26(5), pp. 499-513. <https://dx.doi.org/10.3109/02656731003623590>
- Trujillo, M. and Berjano, E. (2013): Review of mathematical functions used to model the temperature dependence of electrical and thermal conductivities of biological tissue in radiofrequency ablation, *Int. J. of Hyperthermia*, Vol. 29(6), pp. 590-597. <https://dx.doi.org/10.3109/02656736.2013.807438>
- Sung, C.K., Kim, H.B., Jung, J.H., Baik, K.Y., Moon, K.W., Kim, H.S., Yi, J.H. and Chung, J.H. (2016): Historical and mathematical analysis of the irreversibly electroporated liver tissue, *Technology in Cancer Research and Treatment*, Vol. 16(4), pp. 488-496. <https://dx.doi.org/10.1177/1533034616640642>
- Mahlbacher, G., Curtis, L.T., Lowengurb, J. and Frieboes, H.B. (2018): Mathematical modeling of tumor-associated macrophage interactions with the cancer microenvironment, *J. for Immunotherapy of Cancer*, Vol. 6(1), pp. 1-17. <https://dx.doi.org/10.1186/s40425-017-0313-7>
- Liu, Z., Ahmed, M., Weinstein, Y., Yi, M., Mahajan, R.L. and Goldberg, S.N. (2006): Characterization of the RF ablation-induced ‘oven effect’: The importance of background tissue thermal conductivity on tissue heating, *Int. J. of Hyperthermia*, Vol. 22(4), pp. 327-342. <https://dx.doi.org/10.1080/02656730600609122>
- Adheyjanju, O.O., Al-Angari, H.M. and Sahakian, A.V. (2012): The optimization of needle electrode number and placement for irreversible electroporation of hepatocellular carcinoma, *Radiology and Oncology*, Vol. 46(2), pp. 126-135. <http://dx.doi.org/10.2478/v10019-012-0026-y>
- Pillai, K., Akhter, J., Chua, T.C., Shehata, M., Alzahrani, N., Al-Alem, I., Morris, D.L. (2015): Heat sink effect on tumor ablation characteristics as observed in monopolar radiofrequency, bipolar radiofrequency and microwave, using ex vivo calf liver model, *Medicine*, Vol. 94(9), e580. <https://dx.doi.org/10.1097/MD.0000000000000580>
- Rossmann, C., McCrackin, M.A., Arneson, K.E. and Haemmerich, D. (2017): Temperature-sensitive liposomes combined with thermal ablation: Effects of duration and timing of heating in mathematical models and in vivo, *PLOS ONE*, Vol. 12(6), e0179131. <https://dx.doi.org/10.1371/journal.pone.0179131>
- Tungitkusolmun, S., Staelin, S.T., Haemmerich, D., Tsai, J.Z., Cao, H., Webster, J.G., Lee, F.T. Jr., Mahvi, D.M. and Vorperian, V.R. (2002): Three-dimensional finite-element analyses for radio-frequency hepatic tumor ablation, *IEEE Transactions on Bio-medical Engineering*, Vol. 49(1), pp. 3-9. <http://dx.doi.org/10.1109/10.972834>

- Haemmerich, D. and Webster, J.G. (2005): Automatic control of finite element models for temperature-controlled radiofrequency ablation, *Biomedical Engineering OnLine*, Vol. 4(1), 42. <http://dx.doi.org/10.1186/1475-925X-4-42>
- Kroger, T., Altrögge, I., Preusser, T., Pereira, L., Schmidt, D., Weihusen, A. and Peitgen, H.O. (2006): Numerical simulation of radio frequency ablation with state dependent material parameters in three space dimensions, Springer, *Medical Image Computing and Computer-Assisted Intervention*, Vol. 4191, pp. 380-388. [http://dx.doi.org/10.1007/11866763\\_47](http://dx.doi.org/10.1007/11866763_47)
- Wang, Z., Aarya, I., Gueorguieva, M., Liu, D., Luo, H., Manfredi, L., Wang, L., McLean, D., Coleman, S., Brown, S. and Cuschieri, A. (2012): Image-based 3D modeling and validation of radiofrequency interstitial tumor ablation using a tissue-mimicking breast phantom, *Int. J. of Computer Assisted Radiology and Surgery*, Vol. 7(6), pp. 941-948. <http://dx.doi.org/10.1007/s11548-012-0769-3>
- Payne, S., Flanagan, R., Pollari, M., Alhonnoro, T., Bost, C., O'Neill, D., Peng, T. and Stiegler, P. (2011): Image-based multi-scale modeling and validation of radio-frequency ablation in liver tumors, *Philosophical Transactions A*, Vol. 369(1954), pp. 4233-54. <http://dx.doi.org/10.1098/rsta.2011.0240>
- Zhang, B., Moser, M.A.J., Zhang, E.M., Luo, Y. and Zhang, W. (2015): Numerical analysis of the relationship between the area of target tissue necrosis and the size of target tissue in liver tumor with pulsed radiofrequency ablation, *Int. J. of Hyperthermia*, Vol. 31(7), pp. 715-725. <http://dx.doi.org/10.3109/02656736.2015.1058429>
- Mellal, I., Kengne, E., Guemhioui, K.E. and Lakhssassi, A. (2016): 3D modeling using the finite element method for directional removal of a cancerous tumor, *Journal of Biomedical Sciences*, Vol. 5(4), pp. 1-8. <http://dx.doi.org/10.4172/2254-609X.100042>
- Fang, Z., Zhang, B., Moser, Z., Zhang, E. and Zhang, W. (2018): Design of a novel electrode of radiofrequency ablation for large tumor: A finite element study, *J. of Engineering and Science in Medical Diagnostics and Therapy*, Vol. 1(1), 011001-6. <http://dx.doi.org/10.1115/1.4038129>
- Wang, H., Wu, Z., Cui, D., Shi, Y., Zhai, B. (2023): Radiofrequency ablation of hepatocellular carcinoma: current status, challenges, and prospects, *Liver Research*, 7(2), pp. 108-115. <https://dx.doi.org/10.1016/j.livres.2023.05.002>
- Qu, Y., Chen, Z. and Li, X. (2023): Quantitative review of anesthesia in liver tumor ablation: A bibliometric study from 1999 to 2022, *Medical Science Monitor*, 29, e939607-1–e939607-14. <https://dx.doi.org/10.12659/MSM.939607>
- Başkak, F., Aksu, S.A., Kılıçoğlu, Z.G., Tilki, M. (2023): Local recurrence after thermal ablation therapy of malignant hepatic tumors, *Comprehensive Medicine*, 15(4), pp. 326-334. <https://dx.doi.org/10.14744/cm.2023.64935>
- Hepatic Tumor Ablation, COMSOL Multiphysics 4.3 Model Library.
- Surita, M., Marwaha, A. and Marwaha, S. (2012): Finite element analysis for optimizing antenna for microwave coagulation therapy, *J. of Engineering Science and Technology*, Vol. 7(4), pp. 462-470.
- Dechaumphai, P. (1999): *Finite Element Method in Engineering*, 2nd edition, Chulalongkorn University Press, Bangkok.
- Nasrin, R., Hossain, A. and Zahan, I. (2020): Blood flow analysis inside a stenotic artery using Power-Law fluid model”, *Research and Development in Material Sci.*, Vol. 13(1), pp. 1360-1368. <http://dx.doi.org/10.31031/RDMS.2020.13.000803>
- Biswas, C., Nasrin, R. and Ahmad, M.S. (2022): Numerical analogy of bioheat transfer and microwave cancer therapy for liver tissue, *Heat Transfer*, 51(7), pp. 6403-6430. <http://dx.doi.org/10.1002/htj.22597>